Electronic Supplementary Information

A Pairwise/sandwich-like assembly consisting of a TaO_3 nanomesh and reduced graphene oxide for a pelletized self-supported cathode towards high-areal-capacity Li–S batteries

Chenhui Wang, Nobuyuki Sakai, Yasuo Ebina, Shigeru Suehara, Takayuki Kikuchi, Daiming Tang, Renzhi Ma and Takayoshi Sasaki**

Experimental Section

Reagents: Rubidium carbonate (Rb_2CO_3, 99.9%, Rare Metallic), tantalum oxide (Ta_2O_5, 99.99%, Rare Metallic), hydrochloric acid (concentrated HCl, Kishida Chemical), tetrabutylammonium hydroxide solution (TBAOH, 10 wt%, Wako special grade, FUJIFILM Wako Pure Chemical), graphite (FUJIFILM Wako Pure Chemical), potassium permanganate ($KMnO_4$, FUJIFILM Wako Pure Chemical), sulfuric acid (H_2SO_4, 95.0 wt%, FUJIFILM Wako Pure Chemical), hydrogen peroxide (H_2O_2, 30%, FUJIFILM Wako Pure Chemical), hydrazine monohydrate ($N_2H_4{\cdot}H_2O$, 98 wt%, Kishida Chemical), poly(diallyldimethylammonium) chloride (PDDA, 20 wt% in water, Aldrich), sulfur (S, 99.998%, Aldrich), lithium bis(trifluoromethanesulfonyl)imide (LiTFSI, 99.95%, Aldrich), lithium nitrate ($LiNO_3$, SAJ first grade, Sigma–Aldrich), 1,2-dimethoxyethane (DME, 99.5%, Sigma–Aldrich), 1,3-dioxolane (DOL, 99.8%, Sigma–Aldrich), carbon disulfide (CS_2, 99%, FUJIFILM Wako Pure Chemical), lithium foil (Li, 99.8%, Alfa Aesar), lithium sulfide (Li_2S, 99.98%, Aldrich), tetraglyme (99.9%, Sigma–Aldrich), activated carbon (Strem Chemicals), carbon nanotubes (CNTs, 95%, Aldrich) were obtained. These materials were used as purchased.

Preparation of a colloidal suspension of TaO_3 nanomeshes and their restacked form: TaO_3 nanomesh was prepared according to our previous report.[1] Briefly, a well-ground mixture of Rb_2CO_3 and Ta_2O_5 (molar ratio = 1.02:1) was heated at 900 °C for 1 h for decarbonation. After cooling, the mixture was ground again and then calcined at 900 °C for 20 h to produce $RbTaO_3$. Then, $RbTaO_3$ (10 g) was immersed in an HCl solution (1 mol dm^{-3}, 1 dm^3) and stirred for 3 days (the acid solution was changed every 24 h by decantation). The obtained powder sample of $HTaO_3{\cdot}1.3H_2O$ (4 g) was dispersed in a tetrabutylammonium hydroxide (TBAOH) aqueous solution (1 dm^3) at a concentration corresponding to the molar ratio of

$TBA^+:H^+ = 1:1$. After shaking for 10 days at 180 rpm, the sample was first centrifuged at 2000 rpm for 10 min to remove an unexfoliated material. The resulting suspension was then centrifuged at 20000 rpm for 30 min to recover TaO_3 nanomesh. After washing with deionized water until the supernatant became neutral, TaO_3 nanomesh was dispersed in water to produce a colloidal suspension of the delaminated TaO_3 nanomeshes as a final product. The restacked form of TaO_3 was obtained by flocculating TaO_3 suspension (0.48 g dm^{-3}, 0.2 dm^3) with PDDA solution (5 g dm^{-3}, 0.2 dm^3), followed by freeze-drying.

Preparation of a colloidal suspension of GO, rGO and PDDA-modified rGO nanosheets and the restacked form of PDDA-modified rGO: Graphene oxide (GO) nanosheets were prepared according to the modified Hummers' method.[2] Briefly, $KMnO_4$ (3 g) was slowly added into a mixture of graphite (1 g) and H_2SO_4 (25 cm^3) in an ice bath, and the temperature was kept below 4 °C. After stirring for 2 h, the mixture was stirred at 35 °C for another 3 h. Then, H_2O (46 cm^3) was added dropwise and stirred for 1 h at 100 °C. H_2O (70 cm^3) and H_2O_2 (10 cm^3) were added in sequence and stirred for 1 h. The mixture was centrifuged (5000 rpm for 30 min) and washed with HCl (1 mol dm^{-3}) three times and then washed with water until the supernatant became neutral. The obtained graphite oxide was exfoliated and dispersed in water by ultrasonic treatment. The resulting suspension was centrifuged at 5000 rpm for 30 min to remove unexfoliated graphite oxide. The top solution was further centrifuged at 20000 rpm for 30 min, and the recovered sediment was dispersed in H_2O to obtain a suspension of GO. To prepare PDDA-modified reduced graphene oxide (rGO), the GO suspension (0.2 g dm^{-3}, 1 dm^3) was mixed with a PDDA solution (20 wt%, 7.5 cm^3) and hydrazine monohydrate (98 wt%, 0.015 cm^3) and kept at 90 °C for 3 h. The sample underwent repeated centrifugation (20000 rpm for 30 min) and washing with water until the supernatant was neutral. By dispersing the sediment in H_2O, a suspension of PDDA-modified rGO was obtained. A suspension of pristine rGO without PDDA modification was prepared by the same method without the addition of PDDA. The restacked form of PDDA-modified rGO was obtained by flocculating rGO suspension (0.1 g dm^{-3}, 0.2 dm^3) with PDDA solution (5 g dm^{-3}, 0.2 dm^3), followed by freeze-drying.

Calculation of the ratio of TaO_3 nanomeshes to rGO for assembly: To maximize the interfacial area of the two types of nanosheets, the mass ratio of rGO to TaO_3 was calculated based on a hypothetical area-matching model.[3] The TaO_3 nanomesh and rGO have in-plane structures, which are characterized by a face-centered rectangular unit cell of a (0.98 nm) × b

(0.87 nm)[1] and a hexagonal unit cell of a (0.25 nm) (the graphene carbon network is taken as the structure of rGO). The 2D weight densities of the graphene (W_{graphene}) and TaO_3 nanomesh (W_{TaO3}) are $2M$ (C)/($a \times a \times \sin 120° \times N_A$) and $8M$ (TaO_3)/($a \times b \times N_A$), respectively, wherein N_A is Avogadro's number and M (C) and M (TaO_3) are the molecular weights of carbon and TaO_3. To attain an area balance of 1:1, the mass ratio of TaO_3 to rGO is estimated as $W_{TaO3} / W_{\text{graphene}} = 4.8$.

Preparation of the self-assembled composite of TaO_3/rGO and randomly restacked form of TaO_3/rGO: The self-assembled composite (S-TaO_3/rGO) was fabricated by the flocculation method.[4] The suspensions of PDDA-modified rGO (0.1 g dm^{-3}, 0.2 dm^3) and TaO_3 (0.48 g dm^{-3}, 0.2 dm^3) were dropwise added into water at the same speed with stirring. The obtained flocculate was recovered by centrifugation at 5000 rpm for 10 min, washed with deionized water three times, and finally freeze-dried. On the other hand, for preparation of the control sample, the randomly restacked form (R-TaO_3/rGO), the suspensions of TaO_3 nanomesh (0.48 g dm^{-3}, 0.2 dm^3) and pristine rGO (0.1 g dm^{-3}, 0.2 dm^3) were directly poured into a PDDA solution (10 g dm^{-3}, 0.2 dm^3). After centrifugation at 5000 rpm for 30 min, the sediment from the dispersion was freeze-dried.

Material characterization: The lateral size and thickness of nanosheets were examined by AFM (Hitachi, Scanning Probe Microscope AFM5000II). Powder XRD data were collected by a Rigaku Ultima IV diffractometer with a Cu Kα radiation source ($\lambda = 0.15405$ nm). In-plane XRD measurements were conducted with synchrotron radiation ($\lambda = 0.11991(2)$ nm) at the BL-6C of the Photon Factory in High Energy Accelerator Research Organization (KEK). Zeta potential measurements were performed by a zeta-potential and particle size analyzer (Otsuka Electronics Co., Ltd. ELSZ-2). The TG-DTA analysis was carried out by a Rigaku TG-DTA8122. The micro- and nanostructures of the materials were observed by STEM (JEM-2000ARM), TEM (JEM-3000F) and SEM (JSM-6700F) equipped with energy-dispersive X-ray spectroscopy (EDS). The optical absorption spectra were recorded with an ultraviolet-visible spectrophotometer (UV-Vis, Hitachi U-4100). Raman spectra were recorded by a Raman spectrometer (HORIBA Jobin Yvon, T64000).

DFT simulation: All DFT simulations using the VASP package were conducted under the generalized gradient approximation by the Perdew-Burke-Ernzerhof (PBE) exchange-correlation functional with an empirical van der Waals (vdW) interaction correction by

Grimmes (so-called, the semi-empirical PBE-D3 method).[5,6] A wavefunction expansion cutoff energy of 500 eV and Gamma-point sampling in the Brillouin zone integration were employed in this work. In this simulation, a TaO_3 nanomesh model with surface proton, i.e., TaO_3H, was used, because a charge-neutral state of the nanomesh can be assumed in an experimental environment. After screening calculations for finding the most probable surface proton configuration, a protonated nanomesh model, $Ta_{32}O_{96}H_{32}$, was obtained as shown in Fig. S6. A penetration simulation cell consists of the PBE-D3 optimized $Ta_{32}O_{96}H_{32}$ nanomesh single layer and a > 20 Å-thick vacuum layer for removing the effect of periodic boundary conditions imposed by the present DFT calculation. It should be noted that the present TaO_3 nanomesh model has two penetration paths for the B channel due to the surface proton configuration variation. For the penetration barrier and MEP searching, the five NEB images were used with the fixed TaO_3 nanomesh structure shown in Fig. S6.

Simulation of XRD profile: The XRD patterns were simulated by summing scattering amplitudes for all the atomic pairs in the structure based on the following Debye's equation,[7]

$$\mathrm{I} = \sum_{\mathrm{i}=1}^{\mathrm{N}} \sum_{\mathrm{j}=1}^{\mathrm{N}} \mathrm{f_i f_j} \frac{\sin \mathrm{Qr_{ij}}}{\mathrm{Qr_{ij}}}$$

where N denotes the number of atoms, f_i, f_j are the scattering atomic factors for the *i*th and *j*th atoms, r_{ij} is a distance between them, and Q is the scattering vector (= $4\pi\sin\theta/\lambda$). The calculation was carried out on structure models composed of 2D sheets of TaO_3 and rGO having a lateral size of 100×100 nm^2. The atomic positions were calculated based on the structures of $RbTaO_3$[8] and graphene.

Preparation of the self-supported host electrodes and self-supported sulfur-loaded cathodes: Self-supported host electrodes were fabricated by the pelletizing method. Host materials (the restacked form of rGO, the randomly restacked form of R-TaO_3/rGO and the pair/sandwich-like assembly of S-TaO_3/rGO) were put into a circular mold with a diameter of 10 mm and then pelletized into the self-supported host electrodes at a pressure of 2 MPa for 10 s. The prepared self-supported host electrodes were assembled into a Li_2S_6 symmetrical battery and Li_2S_8 battery for electrochemical tests. Self-supported sulfur-loaded cathodes were prepared by the impregnation method, as follows. A sulfur solution was prepared by dissolving sulfur (20 mg) into CS_2 (1 cm^3) at room temperature. Then, the self-supported host electrodes were immersed in the prepared sulfur solution. After the volatilization of CS_2, self-supported sulfur-loaded cathodes were obtained. The loading amount of sulfur was controlled by adjusting the applied volume of the sulfur solution as well as the thickness of the pellets so that the sulfur contents in the cathodes were controlled at around 50%.

Electrochemical measurements as Li-S batteries: Electrochemical tests were conducted on the CR2032 coin cells assembled in an argon-filled glove box. Self-supported sulfur-loaded electrodes, Celgard 2325, lithium foil and an electrolyte of 1 mol dm^{-3} of LiTFSI with 2 wt% of $LiNO_3$ in DME/DOL (1:1 in volume) were used as the cathodes, separator, anodes and electrolyte, respectively, of the Li-S batteries. The electrochemical tests were conducted on an electrochemical workstation (Solartron, 1280B). The charge/discharge performance of the batteries was evaluated by a battery testing system (Hokuto, HJ1001SD8) in the potential range of 1.7-2.8 V. The ratios between electrolyte and sulfur (E/S) were 15.2 μL mg^{-1}, 7.6 μL mg^{-1} and 5.1 μL mg^{-1} for the Li-S batteries with the sulfur loading of 5, 10 and 15 mg cm^{-2}, respectively.

Study of the kinetics of lithium polysulfides conversion: The Li_2S_6 electrolytes with 0.2 mol dm^{-3} Li_2S_6 + 1 mol dm^{-3} LiTFSI + 2 wt% $LiNO_3$ in DOL/DME (1:1 in volume) were prepared by adding S and Li_2S at a molar ratio of 5:1, LiTFSI, and $LiNO_3$ in DOL/DME (1:1 in volume) and stirring for 48 h at 60 °C. The Li_2S_6 symmetric cells were assembled with the self-supported host electrodes (rGO, R-TaO_3/rGO and S-TaO_3/rGO) acting as both the working and counter electrodes, a Celgard 2325 separator and a Li_2S_6 electrolyte. CV and EIS tests were conducted on the Li_2S_6 symmetrical cells by an electrochemical workstation (Solartron, 1280B).

Study of Li_2S nucleation: S and Li_2S with the molar ratio of 7:1, as well as LiTFSI, were added into tetraglyme to prepare the Li_2S_8 catholyte with 0.3 mol dm^{-3} Li_2S_8 + 1.0 mol dm^{-3} LiTFSI in tetraglyme by stirring at 60 °C for 48 h. The Li_2S_8 cell was assembled with the self-supported host electrode, lithium foil, Celgard 2325, Li_2S_8 electrolyte and tetraglyme as the cathode, anode, separator, catholyte and anolyte, respectively, to study Li_2S nucleation kinetics. The Li_2S_8 coin cells were first galvanostatically discharged to 2.06 V (vs. Li^+/Li) at 112 μA and then kept at 2.05 V on the electrochemical workstation (Solartron, 1280B).

Polysulfides permeability test: Two L-type chambers were assembled into an H-type vessel separated by a Celgard 2325 or TaO_3-modified Celgard 2325 to assemble an H-type vessel. The TaO_3-modified Celgard 2325 with the loading of TaO_3 (~0.1 mg cm^{-2}) was prepared by vacuum filtration. Solutions of 0.005 mol L^{-1} Li_2S_6 in DOL/DME (1:1 in volume) and pure DOL/DME (1:1 in volume) were used to fill the left and right chambers, respectively, for monitoring the sieving capability of TaO_3 toward polysulfides.

Lithium polysulfides adsorption test: Host materials (R-TaO_3/rGO or S-TaO_3/rGO, 15 mg) were added into a Li_2S_6 in DOL/DME (1:1 in volume) solution (0.005 mol dm^{-3}, 4 cm^3). The adsorption capacity of the materials was evaluated by the colour of the solutions and their UV-Vis spectra after mixing.

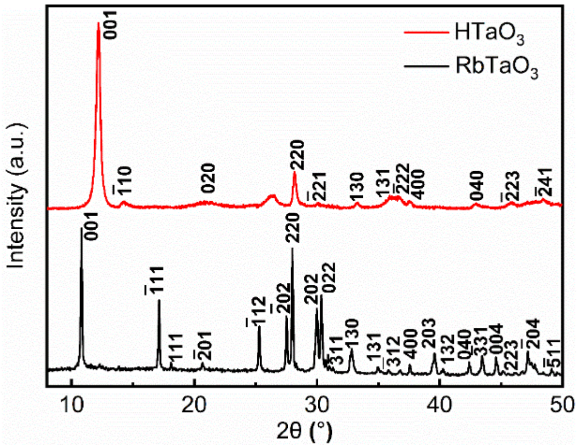

Fig. S1. XRD patterns of $RbTaO_3$ and $HTaO_3 \cdot 1.3H_2O$.

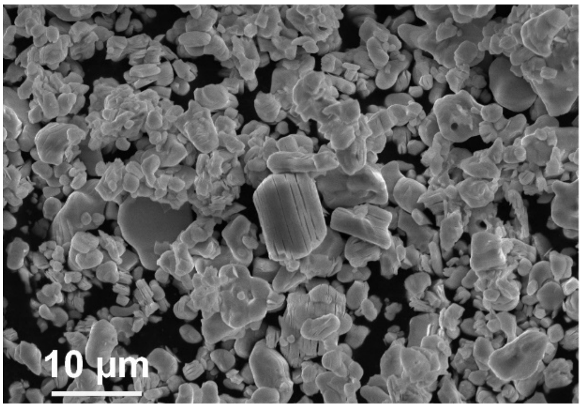

Fig. S2. SEM image of $RbTaO_3$.

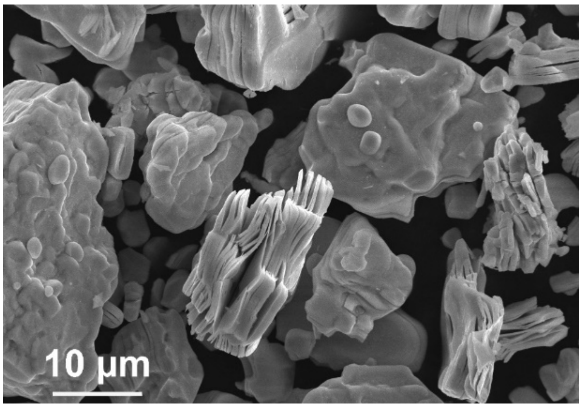

Fig. S3. SEM image of $HTaO_3 \cdot 1.3H_2O$.

Fig. S4. A photograph of a colloidal suspension of TaO_3 nanomesh exfoliated in an aqueous TBAOH solution.

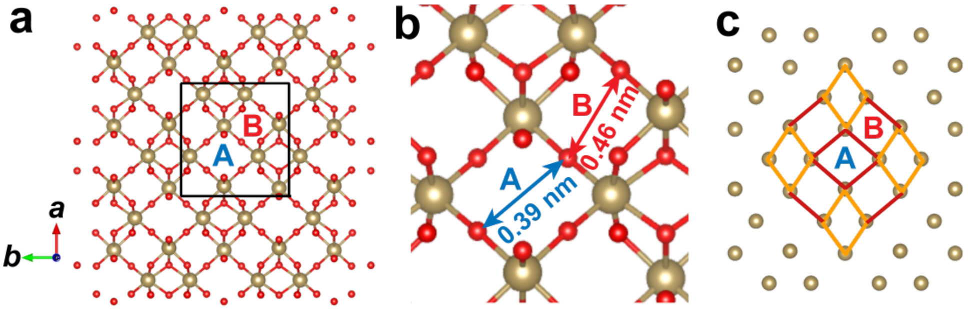

Fig. S5. a) Ball-and-stick structure model of the TaO_3 layer. b) Enlarged view of the black frame part of (a). c) Ta atom positions in the TaO_3 host layer extracted from (a).

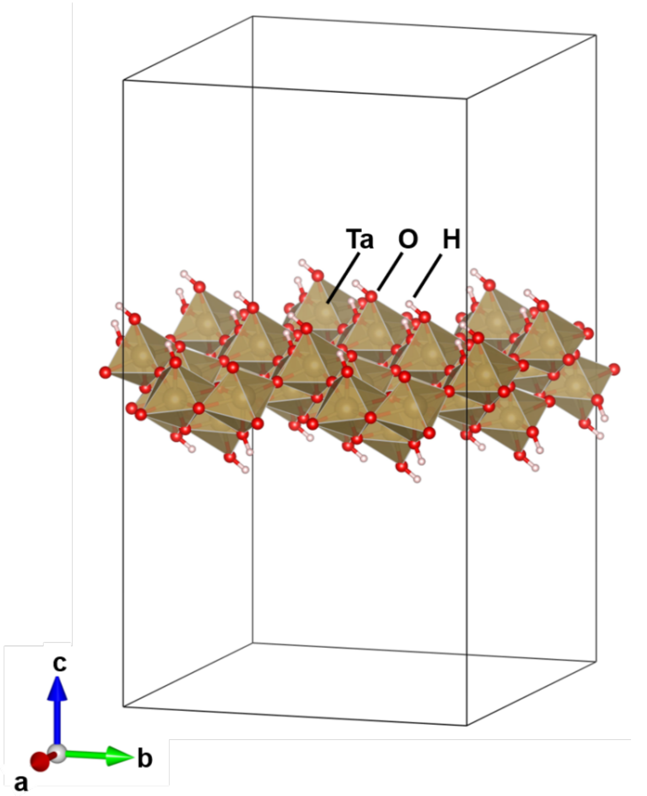

Fig. S6. $Ta_{32}O_{96}H_{32}$ nanomesh simulation cell with a = 19.35 Å, b = 17.10 Å and c = 30.00 Å (Orthorhombic).

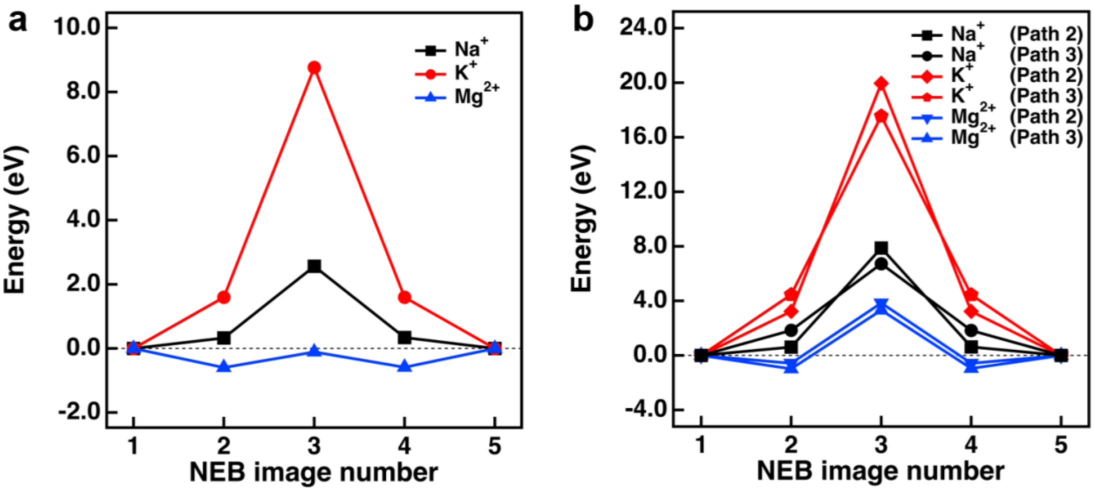

Fig. S7. NEB relative energies for Na^+, K^+ and Mg^{2+} penetration through a) A channel and b) B channel of TaO_3 nanomesh.

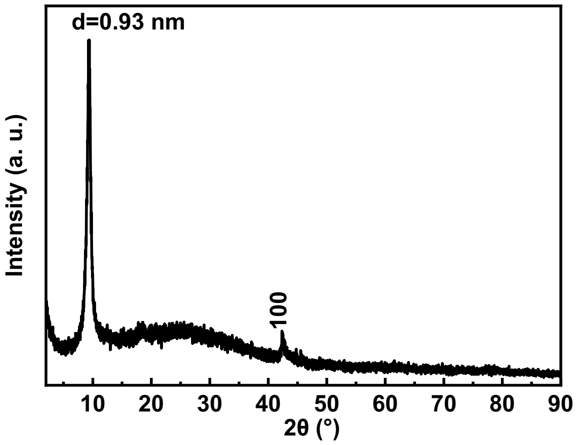

Fig. S8. XRD pattern of graphite oxide.

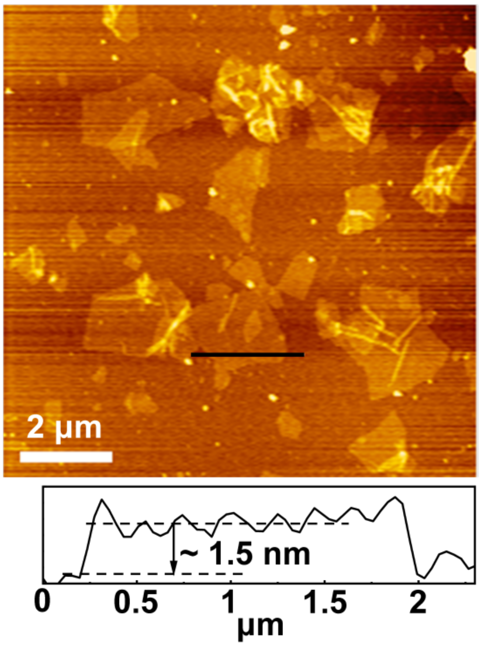

Fig. S9. AFM image and height profile of PDDA-modified rGO nanosheets.

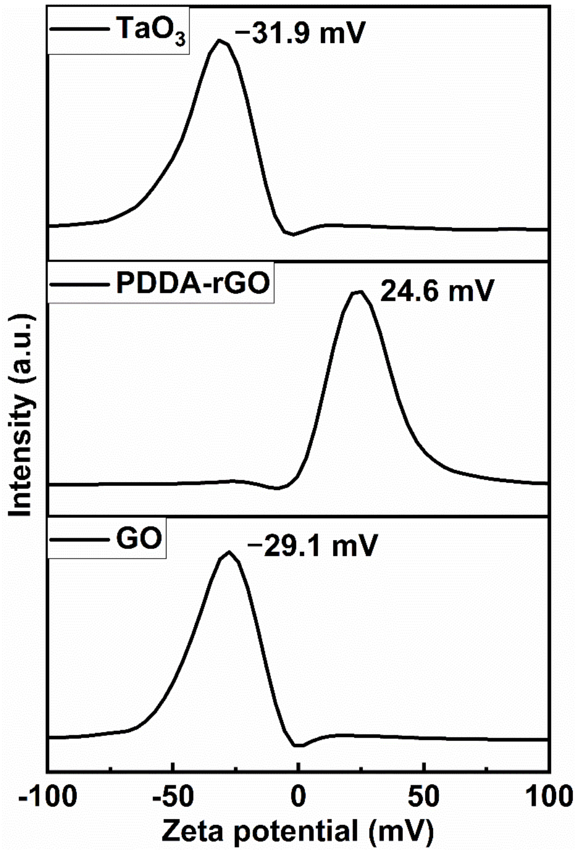

Fig. S10. Zeta potential of suspensions of GO, PDDA-rGO and TaO_3 nanomesh.

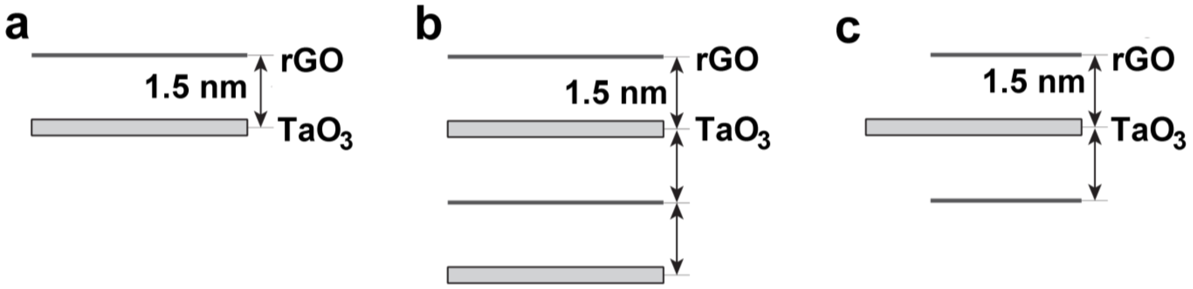

Fig. S11. Structural model for simulating the XRD patterns of the a) single-unit of bilayer rGO/TaO_3, b) double-unit rGO/TaO_3/rGO/TaO_3 and c) sandwich-structured rGO/TaO_3/rGO.

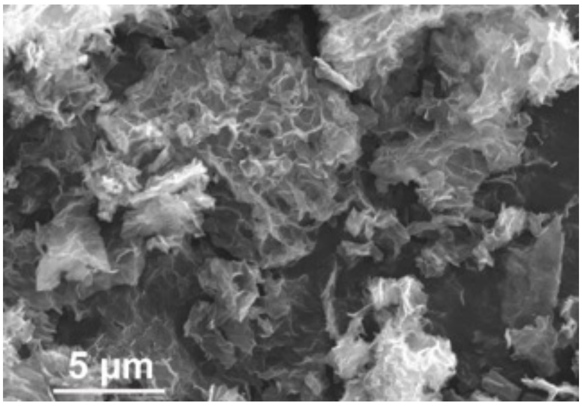

Fig. S12. SEM image of S-TaO$_3$/rGO.

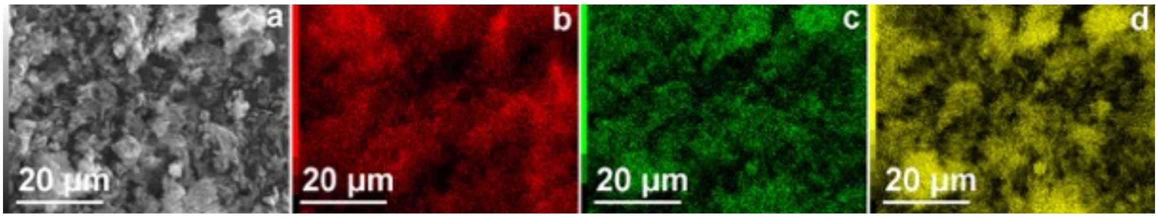

Fig. S13. a) SEM image and EDS mapping of the b) C, c) O and d) Ta in S-TaO$_3$/rGO.

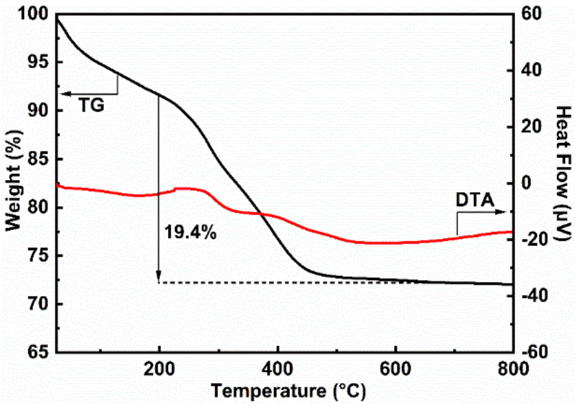

Fig. S14. TG and DTA curves of S-TaO$_3$/rGO.

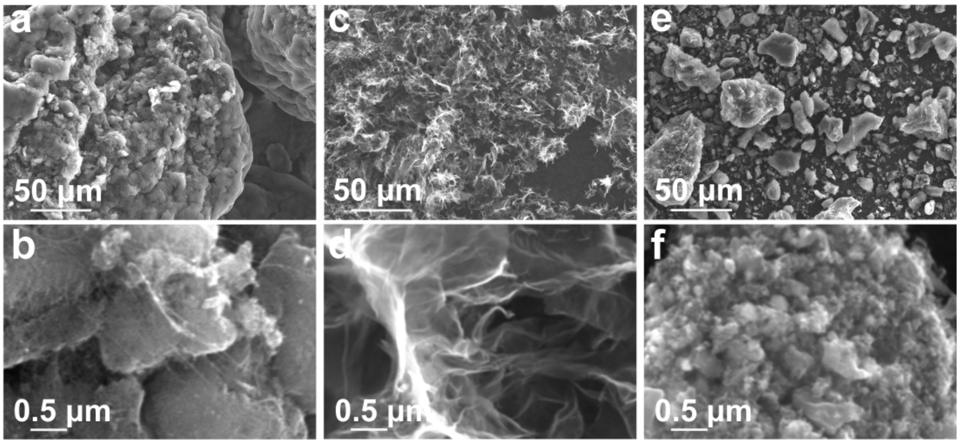

Fig. S15. SEM images of a,b) CNT, c,d) rGO and e,f) activated carbon.

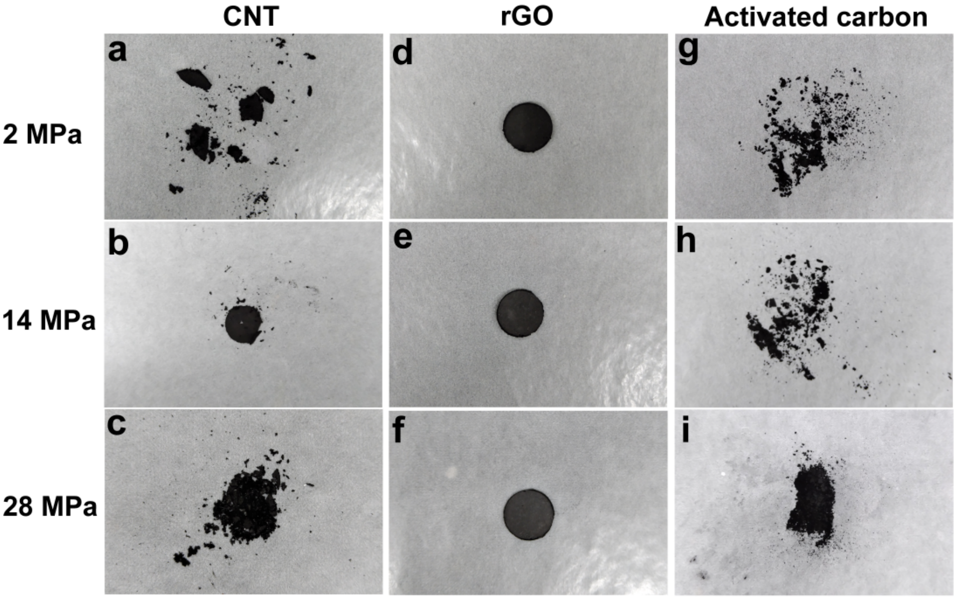

Fig. S16. Pictures of CNT, rGO and activated carbon after applying the indicated pressure in the pelletizing process.

Fig. S17. Thickness of the self-supported rGO pellets fabricated at a) 2 MPa, b) 14 MPa and c) 28 MPa.

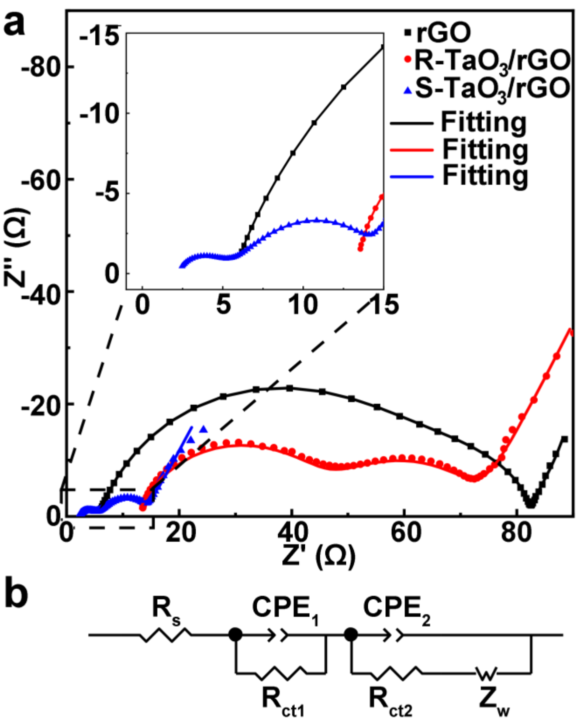

Fig. S18. a) EIS curves of the Li_2S_6 symmetric battery assembled with the rGO, R-TaO_3/rGO and S-TaO_3/rGO self-supported electrodes. Inset: enlarged view of (a). b) Equivalent circuit for the EIS fitting curves in (a).

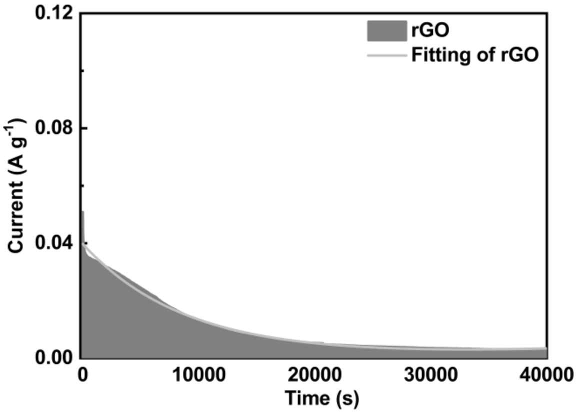

Fig. S19. Fitting of the current vs. time curve for potentiostatic discharge at 2.05 V of the Li_2S_8 battery assembled with the self-supported electrode of rGO. The curve was fitted as the sum of two exponential functions (representing the reduction of Li_2S_8 to Li_2S_6 and the further reduction of Li_2S_6 to shorter-chain lithium polysulfides).

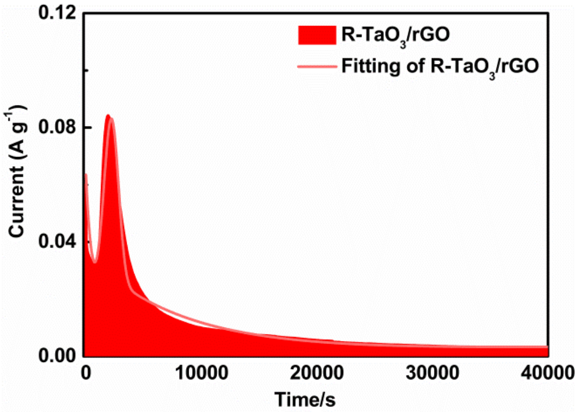

Fig. S20. Fitting of the current vs time curve for potentiostatic discharge at 2.05 V of the Li_2S_8 battery assembled with the self-supported electrode of R-TaO_3/rGO. The curve was fitted as the sum of two exponential functions (representing the reduction of Li_2S_8 to Li_2S_6 and the further reduction of Li_2S_6 to shorter-chain lithium polysulfides) and a peak resulting from the electrodeposition of Li_2S.

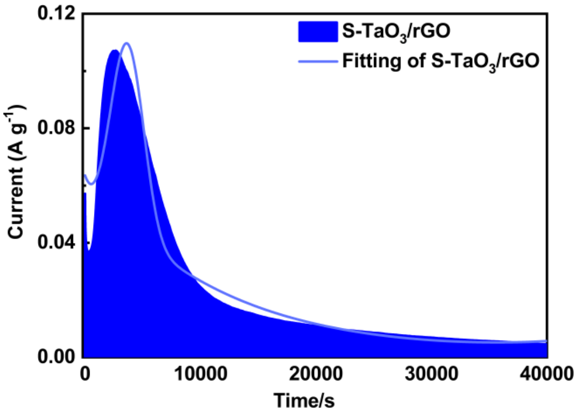

Fig. S21. Fitting of the current vs time curve for potentiostatic discharge at 2.05 V of the Li_2S_8 battery assembled with the self-supported electrode of S-TaO$_3$/rGO. The curve was fitted as the sum of two exponential functions (representing the reduction of Li_2S_8 to Li_2S_6 and the further reduction of Li_2S_6 to shorter-chain lithium polysulfides) and a peak resulting from the electrodeposition of Li_2S.

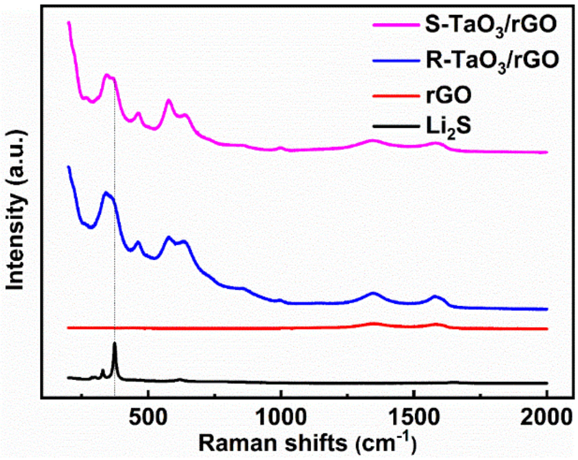

Fig. S22. Raman spectra of the rGO, R-TaO$_3$/rGO and S-TaO$_3$/rGO electrodes after the potentiostatic process. The Raman spectrum of Li_2S is also shown as a reference.

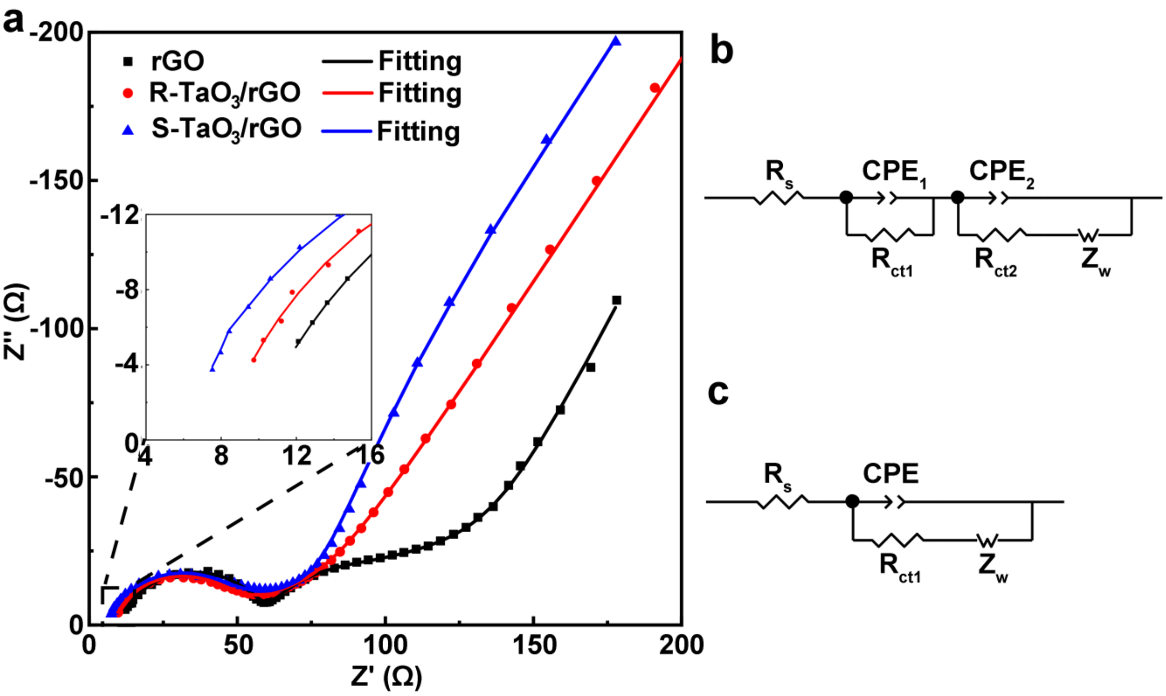

Fig. S23. a) EIS curves of the Li_2S_8 battery assembled with the rGO, R-TaO_3/rGO and S-TaO_3/rGO self-supported electrodes after the potentiostatic process at 2.05 V. Equivalent circuit for the EIS fitting curves in (a) for the Li_2S_8 battery with b) rGO and c) R-TaO_3/rGO and S-TaO_3/rGO.

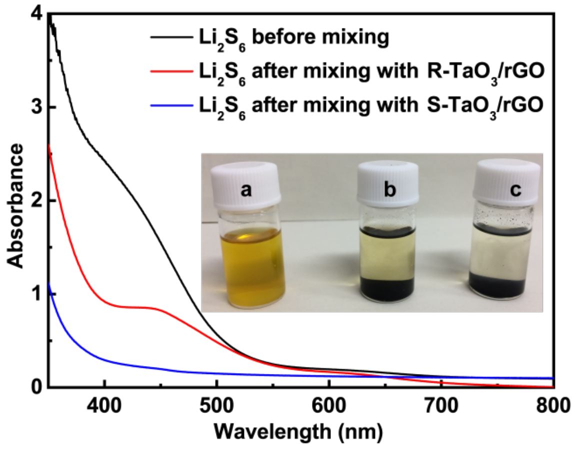

Fig. S24. UV-Vis spectra of the Li_2S_6 electrolyte before and after being mixed with R-TaO_3/rGO and S-TaO_3/rGO. Inset: photograph of 0.005 M Li_2S_6 in DOL/DME (V_{DOL}:V_{DME} = 1:1) solution (4 mL) a) before and after mixing with b) R-TaO_3/rGO (15 mg) and c) S-TaO_3/rGO (15 mg).

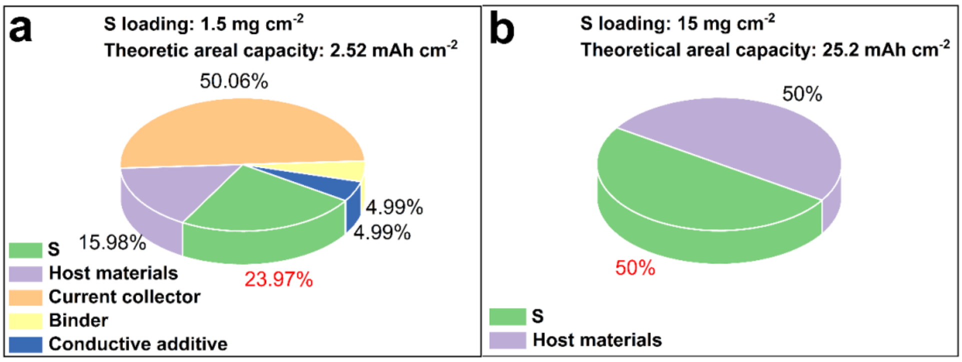

Fig. S25. Mass fraction of ingredients in a) a conventional film cathode and b) the self-supported sulfur-loaded cathodes employed in the present work.

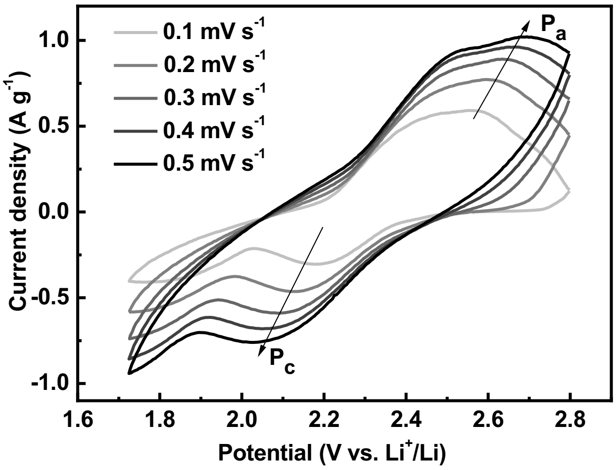

Fig. S26. CV curves of the Li-S battery assembled with the rGO cathode at different scan rates.

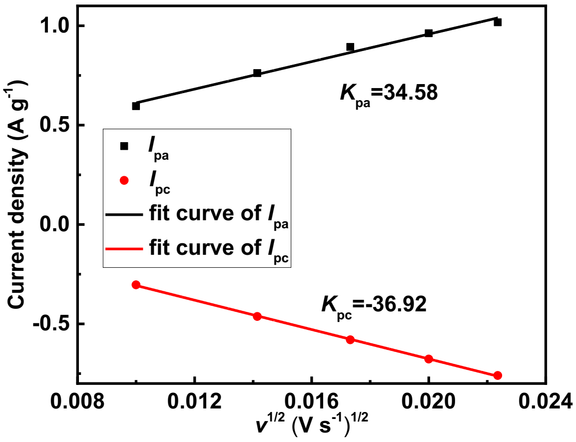

Fig. S27. Linear fit curve of the peak current (I_P) against the $v^{1/2}$ of the Li-S battery assembled with the rGO cathode.

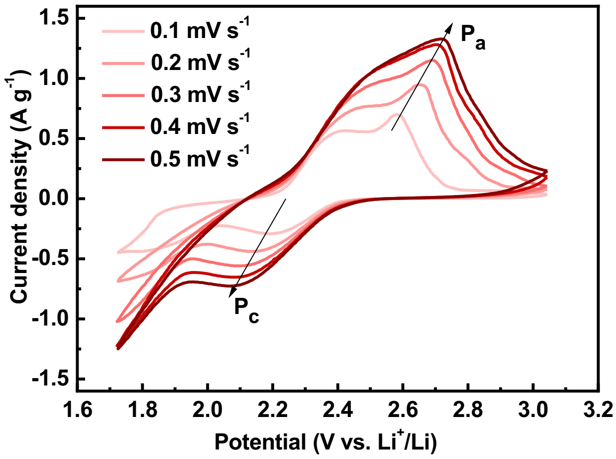

Fig. S28. CV curves of the Li-S battery assembled with the R-TaO$_3$/rGO cathode at different scan rates.

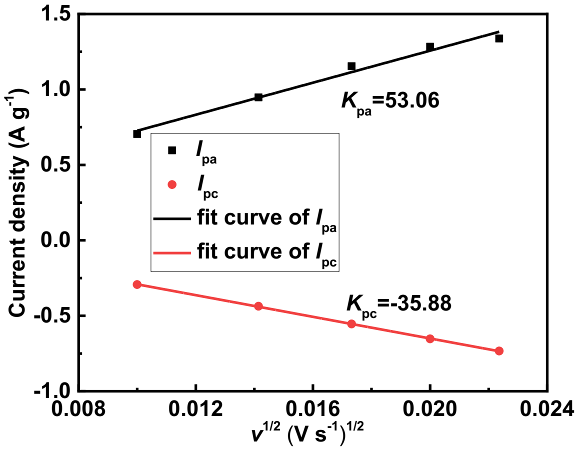

Fig. S29. Linear fit curve of the peak current (I_P) against the $v^{1/2}$ of the Li-S battery assembled with the R-TaO$_3$/rGO cathode.

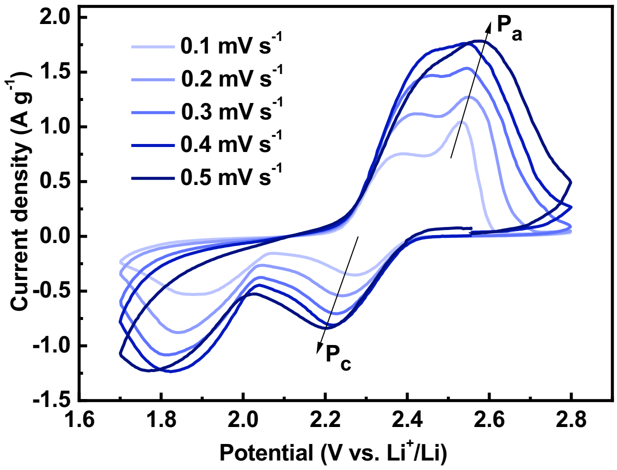

Fig. S30. CV curves of the Li-S battery assembled with the S-TaO$_3$/rGO cathode at different scan rates.

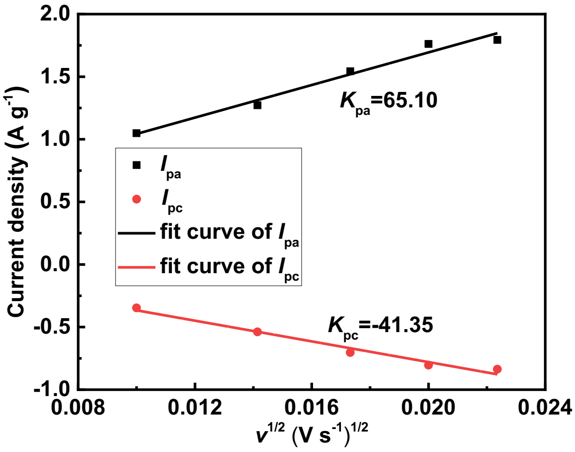

Fig. S31. Linear fit curve of the peak current (I_P) against the $v^{1/2}$ of the Li-S battery assembled with the S-TaO$_3$/rGO cathode.

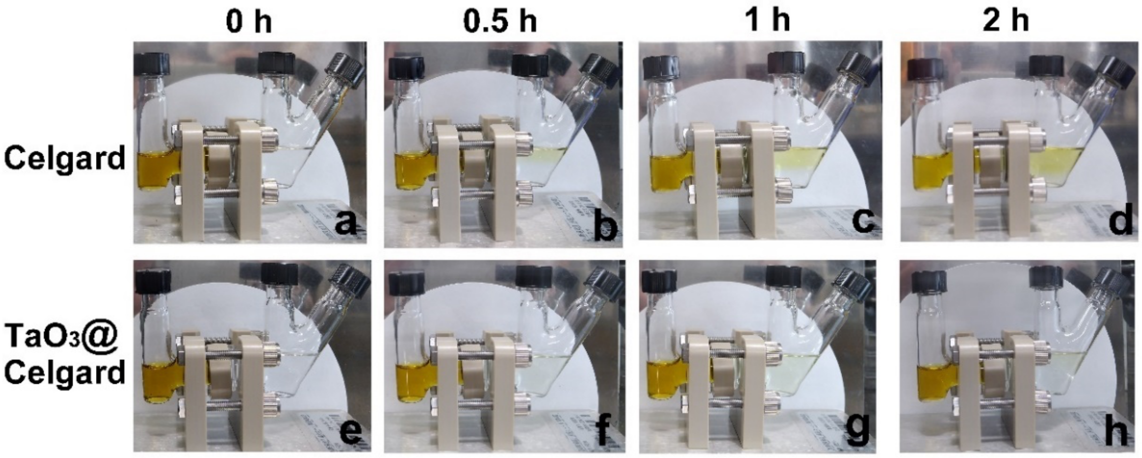

Fig. S32. Time course of permeability of Li$_2$S$_6$ across the Celgard separator and that modified with TaO$_3$ nanomesh: at a,e) 0 h, b,f) 0.5 h, c,g) 1 h and d,h) 2 h.

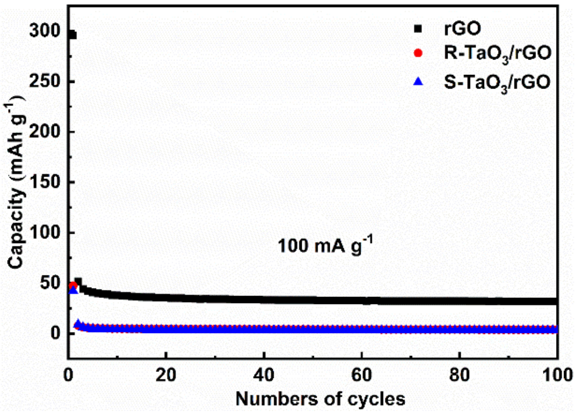

Fig. S33. Capacity of the Li-S batteries assembled with the self-supported cathodes of rGO, R-TaO$_3$/rGO and S-TaO$_3$/rGO without the loading of sulfur at 100 mA g^{-1}.

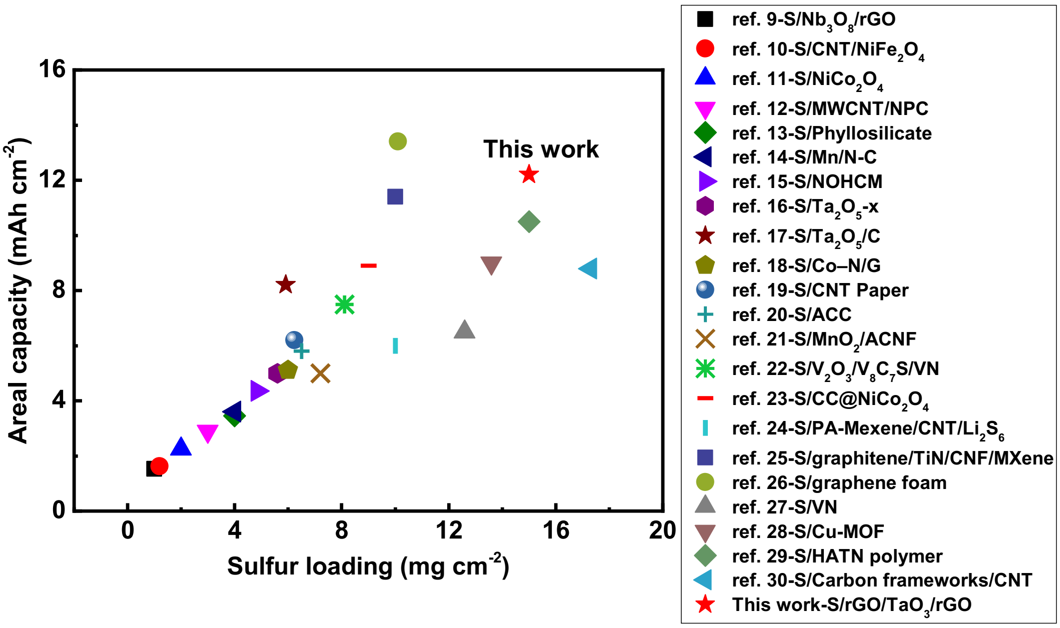

Fig. S34. Comparison of the areal capacity and sulfur loading in this work with those reported in the literatures.[9-30]

References

1. K. Fukuda, I. Nakai, Y. Ebina, R. Ma and T. Sasaki, *Inorg. Chem.*, 2007, **46**, 4787-4789.
2. S. Park, J. An, R. D. Piner, I. Jung, D. Yang, A. Velamakanni, S. T. Nguyen and R. S. Ruoff, *Chem. Mater.*, 2008, **20**, 6592-6594.
3. L. Li, R. Ma, Y. Ebina, K. Fukuda, K. Takada and T. Sasaki, *J. Am. Chem. Soc.*, 2007, **129**, 8000-8007.
4. X. Cai, T. C. Ozawa, A. Funatsu, R. Ma, Y. Ebina and T. Sasaki, *J. Am. Chem. Soc.*, 2015, **137**, 2844-2847.
5. J. P. Perdew, K. Burke and M. Ernzerhof, *Phys. Rev. Lett.*, 1996, **77**, 3865-3868.
6. S. Grimme, J. Antony, S. Ehrlich and H. Krieg, *J. Chem. Phys.*, 2010, **132**, 154104.
7. P. Debye, *Ann. Phys.*, 1915, **351**, 809-823.
8. M. Serafin and R. Hoppe, *Angew. Chem. Int. Ed.*, 1978, **17**, 354-355.
9. C. Wang, N. Sakai, Y. Ebina, T. Kikuchi, M. R. Snowdon, D. Tang, R. Ma and T. Sasaki, *J. Mater. Chem. A*, 2021, **9**, 9952-9960.
10. Q. Fan, W. Liu, Z. Weng, Y. Sun and H. Wang, *J. Am. Chem. Soc.*, 2015, **137**, 12946-12953.
11. Y.-T. Liu, D.-D. Han, L. Wang, G.-R. Li, S. Liu and X.-P. Gao, *Adv. Energy Mater.*, 2019, **9**, 1803477.
12. H.-S. Kang and Y.-K. Sun, *Adv. Funct. Mater.*, 2016, **26**, 1225-1232.
13. W. Chen, T. Lei, W. Lv, Y. Hu, Y. Yan, Y. Jiao, W. He, Z. Li, C. Yan and J. Xiong, *Adv.*

Mater., 2018, **30**, 1804084.

14. Y. Liu, Z. Wei, B. Zhong, H. Wang, L. Xia, T. Zhang, X. Duan, D. Jia, Y. Zhou and X. Huang, *Energy Storage Mater.*, 2021, **35**, 12-18.
15. X. Zhou, J. Tian, Q. Wu, J. Hu and C. Li, *Energy Storage Mater.*, 2020, **24**, 644-654.
16. Z. Zhang, D. Luo, G. Li, R. Gao, M. Li, S. Li, L. Zhao, H. Dou, G. Wen, S. Sy, Y. Hu, J. Li, A. Yu and Z. Chen, *Matter*, 2020, **3**, 920-934.
17. J. Choi, T.-G. Jeong, D. Lee, S. H. Oh, Y. Jung and Y.-T. Kim, *J. Power Sources*, 2019, **435**, 226707.
18. Z. Du, X. Chen, W. Hu, C. Chuang, S. Xie, A. Hu, W. Yan, X. Kong, X. Wu, H. Ji and L.-J. Wan, *J. Am. Chem. Soc.*, 2019, **141**, 3977-3985.
19. Z. Yuan, H.-J. Peng, J.-Q. Huang, X.-Y. Liu, D.-W. Wang, X.-B. Cheng and Q. Zhang, *Adv. Funct. Mater.*, 2014, **24**, 6105-6112.
20. R. Elazari, G. Salitra, A. Garsuch, A. Panchenko and D. Aurbach, *Adv. Mater.*, 2011, **23**, 5641-5644.
21. H. Xu, L. Qie and A. Manthiram, *Nano Energy*, 2016, **26**, 224-232.
22. L. Zhang, Y. Liu, Z. Zhao, P. Jiang, T. Zhang, M. Li, S. Pan, T. Tang, T. Wu, P. Liu, Y. Hou and H. Lu, *ACS Nano*, 2020, **14**, 8495-8507.
23. S. Chen, J. Zhang, Z. Wang, L. Nie, X. Hu, Y. Yu and W. Liu, *Nano Lett.*, 2021, **21**, 5285-5292.
24. B. Zhang, C. Luo, G. Zhou, Z.-Z. Pan, J. Ma, H. Nishihara, Y.-B. He, F. Kang, W. Lv and Q.-H. Yang, *Adv. Funct. Mater.*, 2021, **31**, 2100793.
25. R. Hou, S. Zhang, Y. Zhang, N. Li, S. Wang, B. Ding, G. Shao and P. Zhang, *Adv. Funct. Mater.*, 2022, **32**, 2200302.
26. G. Zhou, L. Li, C. Ma, S. Wang, Y. Shi, N. Koratkar, W. Ren, F. Li and H.-M. Cheng, *Nano Energy*, 2015, **11**, 356-365.
27. R. Liu, W. Liu, Y. Bu, W. Yang, C. Wang, C. Priest, Z. Liu, Y. Wang, J. Chen, Y. Wang, J. Cheng, X. Lin, X. Feng, G. Wu, Y. Ma and W. Huang, *ACS Nano*, 2020, **14**, 17308-17320.
28. B. Liu, J. F. Torres, M. Taheri, P. Xiong, T. Lu, J. Zhu, Y. Liu, G. Yu and A. Tricoli, *Adv. Energy Mater.*, 2022, **12**, 2103444.
29. X. Wang, Y. Yang, C. Lai, R. Li, H. Xu, D. H. S. Tan, K. Zhang, W. Yu, O. Fjeldberg, M. Lin, W. Tang, Y. S. Meng and K. P. Loh, *Angew. Chem. Int. Ed.*, 2021, **60**, 11359-11369.
30. N. Wang, X. Zhang, Z. Ju, X. Yu, Y. Wang, Y. Du, Z. Bai, S. Dou and G. Yu, *Nat. Commun.*, 2021, **12**, 4519.